Energetic control of redox-active polymers towards safe organic bioelectronic materials

Alexander Giovannitti, Reem B. Rashid, Quentin Thiburce, Bryan D. Paulsen, Camila Cendra, Karl Thorley, Davide Moia, J. Tyler Mefford, David Hanifi, Du Weiyuan, Maximilian Moser, Alberto Salleo, Jenny Nelson, Iain McCulloch, and Jonathan Rivnay*

Dr. Alexander Giovannitti, Dr. Karl Thorley, Maximilian Moser, Prof. Iain McCulloch
Department of Chemistry, Imperial College London, London, SW7 2AZ, UK.
Corresponding author: ag19@stanford.edu

Dr. Alexander Giovannitti, Dr. Davide Moia, Prof. Jenny Nelson
Department of Physics, Imperial College London, London, SW7 2AZ, UK

Dr. Du Weiyuan, Prof. Iain McCulloch
King Abdullah University of Science and Technology (KAUST), Physical Sciences and Engineering Division, KAUST Solar Center (KSC), Thuwal 23955-6900, Saudi Arabia

Reem R. Rashid, Dr Bryan D. Paulsen, Prof. Jonathan Rivnay
Simpson Querrey Institute, Northwestern University, Chicago, Illinois 60611, United States
Department of Biomedical Engineering, Northwestern University, 2145 Sheridan Road, Evanston, Illinois 60208, United States

Dr. Alexander Giovannitti, Camila Cendra, Dr. Quentin Thiburce, David Hanifi, Dr. J. Tyler Mefford and Prof. Alberto Salleo
Department of Materials Science and Engineering, Stanford University, CA 94305, USA

Keywords: donor-acceptor copolymer, organic-mixed-ionic-electronic-conductor, electrochemical transistor, oxygen reduction reaction, bioelectronics

Abstract

Avoiding faradaic side reactions during the operation of electrochemical devices is important to enhance the device stability, to achieve low power consumption, and to prevent the formation of reactive side-products. This is particularly important for bioelectronic devices which are designed to operate in biological systems. While redox-active materials based on conducting and semiconducting polymers represent an exciting class of materials for bioelectronic devices, they are susceptible to electrochemical side-reactions with molecular oxygen during device operation. We show that electrochemical side reactions with molecular oxygen occur during OECT operation using high performance, state-of-the-art OECT materials. Depending on the choice of the active material, such reactions yield hydrogen peroxide (H_2O_2), a reactive side-product, which may be harmful to the local biological environment and may also accelerate device degradation. We report a design strategy for the development of redox-active organic semiconductors based on donor-acceptor copolymers that prevent the formation of H_2O_2 during device operation. This study elucidates the previously overlooked side-reactions between redox-active conjugated polymers and molecular oxygen in electrochemical devices for bioelectronics, which is critical for the operation of electrolyte-gated devices in application-relevant environments.

Introduction

Organic semiconductors with polar side-chains have been identified as a promising class of materials for the field of bioelectronics. These materials, also called organic mixed ionic/electronic conductors (OMIECs), can exchange ions with aqueous electrolytes when electronic charge carriers are injected, transported, and stored in the bulk of the material.[1] Recent developments of OMIECs based on redox-active conjugated polymers[2–8] and novel device concepts[9,10] have opened up new pathways for bioelectronic devices including integrated circuits for electroencephalogram (EEG) monitoring[9] or low-power voltage amplifiers based on organic electrochemical transistors (OECTs)[11]. Specifically, the OECT has drawn significant attention in the field of organic bioelectronics. It operates by

electrochemically modulating the conductivity of a redox-active channel material with an electrolyte that is often aqueous, through the application of a gate bias[12]. The electrochemical charging of OMIECs can be described as a capacitive faradaic charging process, meaning that the OMIEC undergoes a change in its oxidation state through an electron transfer with the contact (current collector), while ions from the electrolyte penetrate inside the channel material to compensate the charge carriers on the polymer backbone electrostatically with no change in the inserted ion's oxidation state.[13] OECTs can be operated in either depletion or enhancement mode, depending on the choice of channel (and gate) materials. Depletion-mode devices are initially in their conductive, charged state, under zero gate bias and their conductivity can be decreased by performing electrochemical discharging reactions (de-doping), while enhancement-mode devices begin in an intrinsically low conductivity state and become conductive during electrochemical charging reactions (doping). The latter has the advantage of dissipating less static power when the device is not operated[14], due to low OFF currents – which must be minimized as much as possible. One figure of merit for OECTs is their transconductance $g_m = \partial I_D/\partial V_G$, where I_D is the drain current and V_G is the gate voltage. The g_m accounts for the product of the volumetric capacitance and the mobility of the OMIEC and defines how efficiently the transistor can transduce signals. It depends on the width (W), length (L) and thickness (d) of the transistor's channel where the normalized transconductance $g_{\mathrm{m,norm}} = g_{\mathrm{m}} \frac{L}{Wd}$ is often reported to benchmark OECT materials, accounting for volumetric charging of the channel.[15]

The conducting polymer poly(3,4-ethylenedioxythiophene)poly(styrene-sulfonate) PEDOT:PSS exhibits high performance in depletion-mode OECTs[16] and is the most commonly used material in organic bioelectronics. Recently, efficient OMIECs were developed for enhancement-mode OECTs, which, for the first time, exceeded the performance of PEDOT:PSS[3]. This was achieved by polymer backbone and side-chain engineering to improve electronic and ionic charge transport[2,3]. So far, chemical design strategies for enhancement-mode OECT materials focused mostly on the design of

polymer backbones with low ionization potentials (IPs)[2], resulting in turn-on voltages around 0 V vs. a Ag/AgCl pellet electrode in 0.1 M NaCl aqueous solution, with few studies reporting on the electrochemical redox-stability of the materials during operation.[4,5,17]

Electrochemical redox stability of OMIECs is accomplished when reversible capacitive faradaic charging and discharging reactions occur in the absence of non-capacitive faradaic side-reactions between the OMIEC and the electrolyte (e.g. solvent molecules or ions). The products of such side-reactions may modify the chemical composition of the OMIEC and affect the performance of electrochemical devices.[18] So far, little attention has been paid to non-capacitive faradaic reactions in ambient, oxygen-containing aqueous electrolytes. One example of a non-capacitive faradaic reaction is the electron-transfer reaction from the OMIEC to molecular oxygen, also described as the oxygen reduction reaction (ORR). In the absence of an applied potential and mass transport or ohmic effects, a chemical reaction is expected to occur spontaneously when the chemical potential of the products is lower than the reactants, showing the importance of the relationship between the energy levels of the OMIECs and the products of the ORR.[19] The rate of the reaction is thus dependent on both the IP of the OMIEC and, if protons are involved in the reaction, the pH of the solution.

The ORR yields either H_2O_2 (two-electron process)[20] or water (H_2O) (four-electron process)[21,22], as well as charging (oxidation) of the OMIEC that acts as the catalyst. The four-electron reaction ($O_2 + 2H_2O + 4e^- \rightarrow 4OH^-$, E^0 = 1.23 V vs. reversible hydrogen electrode (RHE), pH ≥ 7) is thermodynamically favorable over the two-electron reaction ($O_2 + H_2O + 2e^- \rightarrow HO_2^- + OH^-$, E^0 = 0.76 V vs. RHE, pH > 7) as shown in Figure 1. However, for some classes of materials, including organic molecules[23], the reduction of oxygen can proceed through different pathways which may terminate at the production of dissolved H_2O_2 instead of the complete reduction to water. The electrochemical overpotential for the ORR is the additional voltage beyond the equilibrium voltage required to drive the reaction at a given rate. The equilibrium potential is a function of temperature

and concentrations of reactants and products (based on the Nernst equation) while the electrochemical overpotential is a function of mass transport, ohmic effects, and electron transfer kinetics related to the interaction strengths of reactants and products with the electrode surface.[24].

Formation of H_2O_2 during device operation is a concern when operating in biological environments since corrosive damage to the device materials, or lipid peroxidation can occur.[25–27] The key factor determining which mechanism preferentially occurs during the ORR is the interaction strength of the hydrogen peroxide intermediate (H_2O_2 or HO_2^-) with the electrode surface. If the peroxide intermediate binds weakly to the electrode surface, as observed for metal-free organic molecules[20,28,29], the rate of desorption is higher than the electro-reduction of peroxide and the reaction terminates at the 2-electron pathway. If peroxide binds strongly, the electro-reduction of peroxide is expected to occur faster than desorption and the reaction terminates at the 4-electron pathway. In this regard, the rate for the ORR of organic molecules was reported to depend on the non-carbon heteroatom composition of the polymer and the pH of the electrolyte. When the reaction proceeds via the 4-electron process, a strong pH dependence was observed[22], while a low pH dependence is observed for the 2-electron process.[23] We note that the role of heteroatom doping in directing the pathway is still unclear, but many works suggest nitrogen functionalities as important for the 4-electron reduction.[22]

This work focuses on the implementation of design rules for OMIECs for electrochemical devices such as OECTs to prevent the ORR and hence the formation of H_2O_2 during device operation. We develop OMIECs based on donor-acceptor copolymers that have large IPs to shift the operational voltages of the OECT such that no ORR occurs in ambient conditions in pH neutral aqueous electrolytes (Figure 1). Specifically, we show the importance of functionalizing the donor unit of the copolymer with electron-donating groups to enhance the electrochemical redox stability of donor-acceptor copolymers in aqueous electrolytes. The proposed design strategy is important for the future development of safe organic bioelectronic devices for in-vivo implementation, and for other

devices such as OECT-based sensors where unintended H_2O_2 formation could limit the accurate detection of analytes.

Optoelectronic and electrochemical properties of the donor-acceptor copolymers

Copolymers based on pyridine-flanked diketopyrrolopyrrole (PyDPP) with bithiophene (T2) or 3,3'-methoxybithiophene (MeOT2) (Figure 2a) were synthesized by a Stille polymerization technique where the choice of the comonomer affects the optoelectronic and electronic properties of the copolymers. The bithiophene glycolated copolymer (p(gPyDPP-T2)) has an IP of 5.3 eV as measured by photoelectron spectroscopy in air (PESA) and 5.5 eV when measured by cyclic voltammetry (CV) (Figure S10, Supporting Information). Employing the MeOT2 unit as the comonomer (p(gPyDPP-MeOT2)) lowered the IP to 5.0 eV as measured by both PESA and CV. An increase of the HOMO energy level was also observed by density functional theory (DFT) calculations (tuned ωB97XD/6-31G*) for short oligomers of PyDPP-T2 and PyDPP-MeOT2 resulting in the calculated HOMO energy levels of 5.36 and 4.92 eV, respectively, which compares well to the experimental IP values. Both copolymers have good solubility in chloroform, enabling facile processing from solution, and thin-films of the copolymers are insoluble in aqueous electrolytes. Mass spectrometry indicates the formation of several repeat units for both copolymers (Figure S7 and S9, Supporting Information), while gel permeation chromatography was inconclusive, indicating unrealistically high molecular weights most likely due to aggregation of the copolymers in solution. Details about the synthesis and characterization of the copolymers are given in Sections 2-4, Supporting Information. The thin-film microstructure of the copolymers in their dry, as-cast conditions was studied by grazing incidence wide-angle X-ray scattering (GIWAXS) measurements. The copolymers show similar edge-on texture and π-stacking distances (3.49 Å for p(gPyDPP-MeOT2) and 3.46 Å p(gPyDPP-T2)), while the lamellar spacing increases from 16.87 Å p(gPyDPP-T2) to 19.19 Å p(gPyDPP-MeOT2), most likely due to comonomer substitution as well as the attachment of a longer side-chain on the PyDPP unit to increase the solubility of the copolymer in organic solvents (Figure S12 and Table S2, Supporting Information).

To study the electrochemical redox reactions of the copolymers in aqueous electrolytes, cyclic voltammetry (CV) measurements and spectroelectrochemical measurements were carried out on thin polymer films in aqueous solution. Figure 2b presents the CV measurements of p(gPyDPP-MeOT2) in 0.1 M aqueous NaCl solution. p(gPyDPP-MeOT2) has an oxidation onset potential of 0.3 V vs. Ag/AgCl and shows high redox stability during 50 charging and discharging cycles between 0 V and 0.7 V vs. Ag/AgCl in aqueous electrolytes. Due to the large IP of p(gPyDPP-T2), the oxidation onset is shifted to higher potentials, measured to be 0.75 V vs. Ag/AgCl (Figure S12a, Supporting Information). Compared to the MeOT2 copolymer, the T2 copolymer displays a low electrochemical redox stability in water-based electrolytes (Figure S13, Supporting Information), making the polymer impractical for applications in electrochemical devices. Since the donor-acceptor copolymers have large electron affinities (EA) (Table S1, Supporting Information), they can also be reduced and charged with electrons. The copolymers show reversible electrochemical reduction reactions with a reduction onset of – 0.65 V vs Ag/AgCl for p(gPyDPP-T2) and – 0.75 V vs Ag/AgCl for p(gPyDPP-MeOT2) (Figure S12, Supporting Information).

To study the charging of polymer thin-films in aqueous electrolytes, we carried out spectroelectrochemical measurements for both copolymers (Figure 2c and Figure S12d, Supporting Information). This technique is most useful for studying the charging and discharging of OMIECs where bias-dependent changes of the absorption spectrum can be related to the degree of charging, providing information about polaron and bipolaron formation.[8,30] It is also applicable to identify degradation processes during electrochemical charging/discharging of OMIECs, where irreversible changes of the absorption spectrum can be related to chemical degradation.[18] As shown in Figure 2c, the ground state absorption peak of p(gPyDPP-MeOT2) decreases upon oxidation of the copolymer while a new absorption peak appears for the hole polaron with a similar absorption spectrum as was previously reported for oxidized DPP copolymer analogs [31,32]. Electrochemically reversible polaron formation up to 0.7 V vs Ag/AgCl is observed for p(gPyDPP-MeOT2). Applying higher potentials reveals bipolaron formation, corresponding to the charging of the polymer repeat

units with two electrical charges, detected by a shift of the isosbestic point observed for the polaron formation as well as an increase of the absorption peak at low energy (> 850 nm) (Figure S14d, Supporting Information). Continuous charging of the copolymer to the bipolaron state results in chemical degradation (Figure S14f, Supporting Information). Due to the low electrochemical redox stability of p(gPyDPP-T2), reversible polaron formation is only observed at a low degree of charging (between 0.75 V and 0.85 V vs Ag/AgCl, Figure 2d), while charging to higher positive potentials results in degradation instead of bipolaron formation (Figure S13b, Supporting Information).

One explanation for the lower redox stability of p(gPyDPP-T2) compared to p(gPyDPP-MeOT2) is revealed by comparing the orbital and charge distribution along the polymer chain (Figure S15, Supporting Information). The MeOT2-unit provides more localization of the wavefunction for the hole polaron than the T2-unit, and is therefore expected to stabilize the hole polaron further and thus increase the redox stability of the copolymer, as we have previously shown for other donor-acceptor copolymers[18]. Additionally, the substitution of the hydrogen atoms in the 3- and 3'-positions of the T2 unit to methoxy-groups (MeOT2 unit) can further shield the backbone from unintended reactions during electrochemical charging (polaron and bipolaron formation).

To give insights into the degradation mechanism during electrochemical charging of the copolymers in aqueous electrolytes, we carried out additional spectroelectrochemical measurements and monitored changes of the Fourier-transform infrared (FT-IR) spectra of the copolymers after applying potentials at which irreversible electrochemical redox reactions occur (Section 11, Supporting Information). For both copolymers, significant changes of the FT-IR spectrum were observed, most pronounced for the C=O stretching vibration of the DPP-core at 1663 cm^{-1} (p(gPyDPP-T2)) and 1654 cm^{-1} (p(gPyDPP-MeOT2)). Additional surface characterizations by X-ray photoelectron spectroscopy (XPS) of pristine and electrochemically-degraded polymer films revealed changes of the N-C=O bond of the DPP unit (Section 12, Supporting Information), indicating degradation of the DPP unit.

Performance of p(gPyDPP-MeOT2) in OECTs

Due to the superior electrochemical redox stability of p(gPyDPP-MeOT2) in aqueous electrolytes compared to the p(gPyDPP-T2) copolymer, we analyzed the performance of the former in p-type enhancement-mode OECTs and compared it to state-of-the-art materials for aqueous electrolyte-gated p-type OECTs, PEDOT:PSS and p(g2T-TT). Figures 3a-b present the output and transfer curves of the p(gPyDPP-MeOT2) OECT where almost no hysteresis is observed. The OECT turns on at gate potentials $V_G < -0.35$ V with an on/off ratio $> 10^5$. The device has a normalized peak transconductance ($g_{m,\ norm}$) of 19.5 S cm^{-1} +/– 2.5 S cm^{-1} (averaged over three devices) at $V_G = -0.7$ V. To compare the performance of p(gPyDPP-MeOT2) to state-of-the-art OECT materials, we measured the hole mobility (μ_h) of p(gPyDPP-MeOT2) in frequency-dependent OECT bandwidth measurements[33] as well as the volumetric capacitance (C^*) by electrochemical impedance spectroscopy (EIS). We recorded a hole mobility of 0.030 +/– 0.007 cm^2 V^{-1} s^{-1} (averaged over three devices) at gate potentials of $V_G = -0.7$ V, which is comparable to mobility values reported for other PyDPP copolymers tested in OFETs[34]. The volumetric capacitance of p(gPyDPP-MeOT2) is 60 F cm^{-3} at an offset potential of 0.7 V vs. Ag/AgCl (Figure S24, Supporting Information), which is on par with values reported for other donor-acceptor copolymers with glycol side-chains[18]. $g_{m,\ norm}$ of p(gPyDPP-MeOT2) OECTs is comparable to other p-type OECTs based on benzodithiophene (BDT) copolymers[2] or propylenedioxythiophene (ProDOT) copolymers[6] but is lower in performance compared to state-of-the-art polymers such as p(g2T-TT)[3] or PEDOT:PSS[16], mostly due to lower values for both μ_h and C^*.[15]

The glycol side chains attached to the backbone enable fast ion transport, resulting in OECT transient response times $\tau_{ON} = 0.77$ ms and $\tau_{OFF} = 0.46$ ms, respectively (Figure S21, Supporting Information). Frequency-dependent transconductance measurements show a cut-off of the device > 100 Hz (Figure S22, Supporting Information), which is of relevance to many electrophysiological processes and can be further improved by downscaling the device dimensions. Devices based on p(gPyDPP-MeOT2) showed good stability under long-term pulsed cycling and continuous charging

conditions, as presented in Figure 3c and Figure S23, Supporting Information. As shown in Figure 3c, no or little change in the ON current is observed after 400 cycles when applying V_G = – 0.5 V, while a decrease of 8 % and 16 % is observed with V_G = – 0.6 V and – 0.7 V, respectively. To highlight the importance of backbone engineering for donor-acceptor polymers, we also tested the polymer p(gPyDPP-T2) in an OECT and observed low device stability during pulsed-cycling tests (Figure S20, Supporting Information).

Faradaic side reactions of OMIECs in ambient conditions

The advantages of current state-of-the-art polymers for aqueous electrolyte-gated OECT materials such as p(g2T-TT)[3] or PEDOT:PSS[16,35] are many-fold, including low operational voltages of the OECTs, as well as a high hole mobility and volumetric capacitance, resulting in a high transconductance. However, when operating these materials in electrochemical devices in ambient conditions, faradaic non-capacitive side-reactions can occur with molecular oxygen that result in the formation of either H_2O_2 or H_2O. The formation of H_2O_2 would affect the performance of the device and could cause harm to biological systems.

To examine the role of the ORR during electrochemical redox reactions of the polymers in ambient conditions and to find out if H_2O_2 or H_2O is formed predominantly, we carried out a set of experiments for PEDOT:PSS and p(g2T-TT), as well as the herein reported p(gPyDPP-MeOT2). First, the ORR was studied by probing the polymer's reactivity towards oxygen. We monitored the oxidation of the polymer by UV-Vis absorption spectroscopy with polymer thin-films immersed in aqueous electrolytes in ambient conditions. For the already oxidized polymers PEDOT:PSS and p(g2T-TT), which accumulate hole polarons due to the ORR when handling the polymers in air or due to potential chemical side-reactions during the synthesis, a potential of – 0.6 V (PEDOT:PSS) or – 0.5 V (p(g2T-TT)) vs. Ag/AgCl was applied to discharge the polymers before monitoring the ORR in open-circuit voltage (OCV) conditions. As shown in Figure 4a, PEDOT:PSS oxidizes rapidly in oxygen-containing aqueous electrolytes and achieves a high degree of charging in less than 10 min, including bipolaron formation. A spontaneous ORR was also observed for p(g2T-TT), albeit at a slower

charging rate and to a lower degree of charging as compared to PEDOT:PSS (Section 15, Supporting Information). In comparison, p(gPyDPP-MeOT2) showed no spectral changes, as shown in Figure 4b and Figures S27, Supporting Information, demonstrating that the copolymer does not undergo ORR in ambient conditions. In order to probe how the oxygen concentration affects the charging rates during ORR with the polymer, we performed additional measurements in aqueous electrolytes with reduced oxygen concentration and observed slower charging rates for both PEDOT:PSS and p(gT2-TT) (Figures S25c and S26c, Supporting Information). That finding shows that de-doped thin films of PEDOT:PSS and p(g2T-TT) undergo spontaneous ORR when immersed in 0.1 M NaCl aqueous solutions in ambient conditions. Since the rate of the ORR highly depends on the pH, we lowered the pH value of the electrolyte and as expected, observed faster charging as well as oxidation to a higher degree of charging for p(g2T-TT) (Figure S28a, Supporting Information), while p(gPyDPP-MeOT2) does not become oxidized at low pH (Figure S28d, Supporting Information). This result emphasizes the low activity of p(gPyDPP-MeOT2) towards a spontaneous electron transfer to molecular oxygen.

We hypothesize that the IPs of the polymers, and therefore their oxidation potentials with respect to the reference electrode in 0.1 M NaCl aqueous solution, determine whether or not the polymers can become oxidized by oxygen to form H_2O_2 (Figure 1). To show this relationship, we measured the oxidation potentials of the polymers by CV in aqueous electrolytes and related them to the potential recorded for ORR on a platinum (Pt) electrode, which is known to be an efficient catalyst for ORR. As shown in Figure 4c, the ORR on Pt electrodes occurs at potentials < 0.2 V vs. Ag/AgCl in 0.1 M NaCl aqueous solution. PEDOT:PSS has the lowest oxidation potential of the polymer series (– 0.8 V vs Ag/AgCl), followed by p(g2T-TT) (– 0.2 V vs. Ag/AgCl) and p(gPyDPP-MeOT2) (0.3 V vs. Ag/AgCl). The large overlap of the cyclic voltammograms measured for PEDOT:PSS and p(g2T-TT) compared to the one measured for ORR on the Pt electrode suggests that an electron-transfer to oxygen is more likely for these polymers than for p(gPyDPP-MeOT2), which shows no or little overlap. A similar trend was also reported for chemical doping of organic semiconductors, showing that the IP of conjugated polymers determines how many charge carriers are transferred from a polymer to the

dopant.[36] For the chemical doping of DPP-based donor-acceptor copolymers with IP > 5.2 eV, specially designed dopants with large electron affinities (EA) are required to achieve a high degree of charging.[37] To properly quantify the relative likelihood of the oxidation reactions of the polymers, the thermodynamic driving forces could be worked out, e.g., using DFT calculations[23,38] if the precise reaction mechanism were known. While the polyanion PSS^- in PEDOT:PSS might affect the rate of oxidation, since it is known to be a good proton conductor[39], we believe that the rapid oxidation of PEDOT:PSS arises from its high-lying HOMO.

To verify whether the ORR predominantly yield H_2O_2 (two-electron process) or H_2O (four-electron process), we carried out rotating ring-disk electrode (RRDE) measurements[40] in oxygen-containing aqueous electrolytes (Section 19, Supporting Information) in 0.1 M aqueous NaCl solution. The RRDE experiment enables the detection of redox-active species at the ring electrode, that are formed during the ORR at the polymer-coated disk electrode. The measurements indicate that at potentials < -0.2 V vs. Ag/AgCl, both PEDOT:PSS and p(g2T-TT) predominantly form H_2O_2 (and water) while p(gPyDPP-MeOT2) would form mostly H_2O (Figure S40, Supporting Information).To further illustrate that the ORR yields H_2O_2, we employed an enzymatic reaction, that is highly selective for the detection of H_2O_2[41] and tested the electrolytes that are used for charging and discharging of the polymers for H_2O_2. We observed H_2O_2 formation for PEDOT:PSS and p(g2T-TT)), whereas no H_2O_2 formation is observed for p(gPyDPP-MeOT2) (Figures S42 and S43, Supporting Information).

To show the impact of the ORR and H_2O_2 formation during OECT operation, we recorded the transfer curves of OECTs of PEDOT:PSS, p(g2T-TT) and p(gPyDPP-MeOT2) and compared the OFF currents of the devices (Figure 4d). The OFF current of p(gPyDPP-MeOT2) is two orders of magnitude lower than that of PEDOT:PSS or p(g2T-TT). The OFF currents of PEDOT:PSS and p(g2T-TT) can be decreased by lowering the oxygen concentration in the electrolyte (decreasing the ORR as shown in Figure S36, Supporting Information) which also lowers the gate current of the OECTs (Figure S38, Supporting Information). To quantify how much H_2O_2 is formed, we measure the gate current during pulsed cycling experiments while varying V_D, V_G and ΔV_G (Section 17, Supporting Information). For

PEDOT:PSS and p(g2T-TT), during continuous device operation under V_G > 0.2 V vs. Ag/AgCl in 0.1 M NaCl aqueous solution, we observed an increase of the injected charge per cycle (obtained by integrating the area-normalized gate current transient response for each gate pulse) proportional to V_D. We also monitored the drain current and observed largest device degradation at potentials at which polymers are in their discharged, low conductivity state (Figures S30-S32, Supporting Information). In comparison, the change in injected charge per cycle for p(gPyDPP-MeOT2) is marginal, as expected, due to the absence of ORR during device operation (Figure S35, Supporting Information). The findings highlight that H_2O_2 formation needs to be avoided to avoid device degradation during long-term measurements.

Finally, we carried out OECT measurements in 0.1 M NaCl aqueous solution with high and low oxygen concentrations (Figure 5) and monitored changes of the OFF current in OECTs at OCV conditions after de-doping the polymer by applying a gate potential. For PEDOT:PSS and p(g2T-TT), a spontaneous turn-on of the device is observed with a faster rise of I_D for PEDOT:PSS compared to p(g2T-TT) (Figures 5a-b), while p(PyDPP-MeOT2) remains in its low conductive state (Figure 5c). This further supports the hypothesis that p(PyDPP-MeOT2) does not become oxidized in ambient conditions and hence does not form H_2O_2 during device operation.

The findings highlight the importance of designing redox-active polymers that have a high performance in OECTs while keeping non-capacitive faradaic side-reactions to a minimum to avoid the formation of reactive side-products such as H_2O_2. This can be achieved by designing OMIECs with IP ≥ 4.9 eV, minimizing chemical and electrochemical side reactions in ambient conditions. While the energy levels of the polymers are important to prevent ORR, the rate of the reaction could also be lowered by designing materials that have large overpotentials for the ORR. If OMIECs are required to develop OECTs with low turn-on voltage vs. Ag/AgCl (e.g. p(g2T-TT)), research efforts should be undertaken to redirect the pathway for ORR to H_2O formation instead of H_2O_2. The findings of this work are also relevant for other applications including energy storage devices, non-volatile

memories or sensor devices where undesired oxidation of the active materials and H_2O_2 formation can affect the retention of the charge[8], modify the charge of a memory state[42], increase device degradation or possibly interfere with the sensing mechanism of biosensors.

Conclusions

In this work, we elucidate electrochemical side-reactions of state-of-the-art p-type OECT materials and show that the materials can undergo an ORR during device operation and form the detrimental side-product H_2O_2. We explore polymer backbones that result in the formation of organic semiconductors with large IPs to avoid ORRs. We show that the engineering of the polymer backbone is important for achieving high electrochemical redox stability in aqueous electrolytes and demonstrate that donor-acceptor polymers are an interesting class of materials for the field of bioelectronics. Although the copolymer displays a lower electronic charge carrier mobility in OECTs compared to state-of-the-art polymers, we believe that the presented chemical design strategy is a viable route for developing next-generation bioelectronic materials, especially for real-life applications where hazardous side-products will need to be avoided and low OFF currents of devices are desired.

Acknowledgments

We thank Eric Daniel Głowacki for fruitful discussions about oxygen reduction reactions. A.G, J.N., and I.M acknowledge funding from EPSRC project EP/G037515/1, EP/N509486/1; D.M and J.N. are grateful for receiving funding from the Supersolar Hub (EP/P02484X/1); and JN acknowledges funding from the European Research Council (ERC) (grant agreement No 742708). A.G. and A.S. acknowledge funding from the TomKat Center for Sustainable Energy at Stanford University. Part of this work was performed at the Stanford Nanofabrication Facilities (SNF) and Stanford Nano Shared Facilities (SNSF), supported by the National Science Foundation as part of the National Nanotechnology Coordinated Infrastructure under award ECCS-1542152. J.R. and B.P acknowledge funding from the National Science Foundation (grant no. NSF DMR-1751308). This work utilized

Northwestern University Micro/Nano Fabrication Facility (NUFAB) and the Keck-II facility of NU*ANCE* Center, which is partially supported by Soft and Hybrid Nanotechnology Experimental (SHyNE) Resource (NSF ECCS-1542205), the Materials Research Science and Engineering Center (DMR-1720139) at the Materials Research Center, the State of Illinois, and Northwestern University. NU*ANCE* is further supported by the International Institute for Nanotechnology (IIN); and the Keck Foundation. Measurements at Stanford Synchrotron Radiation Lightsource, SLAC National Accelerator Laboratory, were supported by the U.S. Department of Energy, Office of Science, Office of Basic Energy Sciences under Contract No. DE-AC02-76SF00515.

Competing Interests statement

The authors declare no competing interests.

References

[1] B. D. Paulsen, K. Tybrandt, E. Stavrinidou, J. Rivnay, *Nat. Mater.* **2020**, *19*, 13.

[2] C. B. Nielsen, A. Giovannitti, D.-T. Sbircea, E. Bandiello, M. R. Niazi, D. A. Hanifi, M. Sessolo, A. Amassian, G. G. Malliaras, J. Rivnay, I. McCulloch, *J. Am. Chem. Soc.* **2016**, *138*, 10252.

[3] A. Giovannitti, D.-T. Sbircea, S. Inal, C. B. Nielsen, E. Bandiello, D. A. Hanifi, M. Sessolo, G. G. Malliaras, I. McCulloch, J. Rivnay, *Proc. Natl. Acad. Sci.* **2016**, *113*, 12017.

[4] A. Giovannitti, C. B. Nielsen, D.-T. Sbircea, S. Inal, M. Donahue, M. R. Niazi, D. A. Hanifi, A. Amassian, G. G. Malliaras, J. Rivnay, I. McCulloch, *Nat. Commun.* **2016**, *7*, 13066.

[5] E. Zeglio, M. M. Schmidt, M. Thelakkat, R. Gabrielsson, N. Solin, O. Inganäs, *Chem. Mater.* **2017**, *29*, 4293.

[6] L. R. Savagian, A. M. Österholm, J. F. Ponder, K. J. Barth, J. Rivnay, J. R. Reynolds, *Adv. Mater.* **2018**, *30*, 1804647.

[7] C. G. Bischak, L. Q. Flagg, K. Yan, C.-Z. Li, D. S. Ginger, *ACS Appl. Mater. Interfaces* **2019**, *11*,

28138.

[8] D. Moia, A. Giovannitti, A. A. Szumska, I. P. Maria, E. Rezasoltani, M. Sachs, M. Schnurr, P. R. F. Barnes, I. McCulloch, J. Nelson, *Energy Environ. Sci.* **2019**, *12*, 1349.

[9] G. D. Spyropoulos, J. N. Gelinas, D. Khodagholy, *Sci. Adv.* **2019**, *5*, eaau7378.

[10] M. J. Donahue, A. Williamson, X. Strakosas, J. T. Friedlein, R. R. McLeod, H. Gleskova, G. G. Malliaras, *Adv. Mater.* **2018**, *30*, 1705031.

[11] V. Venkatraman, J. T. Friedlein, A. Giovannitti, I. P. Maria, I. McCulloch, R. R. McLeod, J. Rivnay, *Adv. Sci.* **2018**, *5*, 1800453.

[12] J. Rivnay, S. Inal, A. Salleo, R. M. Owens, M. Berggren, G. G. Malliaras, *Nat. Rev. Mater.* **2018**, *3*, 17086.

[13] L. Guan, L. Yu, G. Z. Chen, *Electrochim. Acta* **2016**, *206*, 464.

[14] H. Klauk, U. Zschieschang, J. Pflaum, M. Halik, *Nature* **2007**, *445*, 745.

[15] S. Inal, G. G. Malliaras, J. Rivnay, *Nat. Commun.* **2017**, *8*, 1767.

[16] D. Khodagholy, J. Rivnay, M. Sessolo, M. Gurfinkel, P. Leleux, L. H. Jimison, E. Stavrinidou, T. Herve, S. Sanaur, R. M. Owens, G. G. Malliaras, *Nat. Commun.* **2013**, *4*, 2133.

[17] H. Sun, M. Vagin, S. Wang, X. Crispin, R. Forchheimer, M. Berggren, S. Fabiano, *Adv. Mater.* **2018**, *30*, 1704916.

[18] A. Giovannitti, K. J. Thorley, C. B. Nielsen, J. Li, M. J. Donahue, G. G. Malliaras, J. Rivnay, I. McCulloch, *Adv. Funct. Mater.* **2018**, *28*, 1706325.

[19] D. M. de Leeuw, M. M. J. Simenon, A. R. Brown, R. E. F. Einerhand, *Synth. Met.* **1997**, *87*, 53.

[20] E. Mitraka, M. Gryszel, M. Vagin, M. J. Jafari, A. Singh, M. Warczak, M. Mitrakas, M. Berggren, T. Ederth, I. Zozoulenko, X. Crispin, E. D. Głowacki, *Adv. Sustain. Syst.* **2019**, *3*, 1800110.

[21] R. Kerr, C. Pozo-Gonzalo, M. Forsyth, B. Winther-Jensen, *ECS Electrochem. Lett.* **2013**, *2*, F29.

[22] H. W. Kim, V. J. Bukas, H. Park, S. Park, K. M. Diederichsen, J. Lim, Y. H. Cho, J. Kim, W. Kim, T. H. Han, J. Voss, A. C. Luntz, B. D. McCloskey, *ACS Catal.* **2020**, *10*, 852.

[23] V. J. Bukas, H. W. Kim, R. Sengpiel, K. Knudsen, J. Voss, B. D. McCloskey, A. C. Luntz, *ACS Catal.* **2018**, *8*, 11940.

[24] L. Khotseng, in *Electrocatal. Fuel Cells Hydrog. Evol. - Theory to Des.*, IntechOpen, **2018**.

[25] K. Apel, H. Hirt, *Annu. Rev. Plant Biol.* **2004**, *55*, 373.

[26] R. L. Auten, J. M. Davis, *Pediatr. Res.* **2009**, *66*, 121.

[27] V. J. Watt BE, Proudfoot AT, *Toxicol Rev* **2004**, *23*, 51.

[28] W. Fan, B. Zhang, X. Wang, W. Ma, D. Li, Z. Wang, M. Dupuis, J. Shi, S. Liao, C. Li, *Energy Environ. Sci.* **2020**, *13*, 238.

[29] M. Jakešová, D. H. Apaydin, M. Sytnyk, K. Oppelt, W. Heiss, N. S. Sariciftci, E. D. Głowacki, *Adv. Funct. Mater.* **2016**, *26*, 5248.

[30] C. Enengl, S. Enengl, S. Pluczyk, M. Havlicek, M. Lapkowski, H. Neugebauer, E. Ehrenfreund, *ChemPhysChem* **2016**, *17*, 3836.

[31] M. Akbayrak, A. M. Önal, *Polym. Chem.* **2016**, *7*, 6110.

[32] C. Francis, ab D. Fazzi, S. B. Grimm, F. Paulus, S. Beck, de S. Hillebrandt, de A. Pucci de, J. Zaumseil, *J. Mater. Chem. C* **2017**, *5*, 6176.

[33] J. Rivnay, M. Ramuz, P. Leleux, A. Hama, M. Huerta, R. M. Owens, *Appl. Phys. Lett.* **2015**, *106*, 43301.

[34] X. Zhang, C. Xiao, A. Zhang, F. Yang, H. Dong, Z. Wang, X. Zhan, W. Li, W. Hu, *Polym. Chem.* **2015**, *6*, 4775.

[35] D. Khodagholy, T. Doublet, P. Quilichini, M. Gurfinkel, P. Leleux, A. Ghestem, E. Ismailova, T. Hervé, S. Sanaur, C. Bernard, G. G. Malliaras, *Nat. Commun.* **2013**, *4*, 1575.

[36] D. Kiefer, R. Kroon, A. I. Hofmann, H. Sun, X. Liu, A. Giovannitti, D. Stegerer, A. Cano, J. Hynynen, L. Yu, Y. Zhang, D. Nai, T. F. Harrelson, M. Sommer, A. J. Moulé, M. Kemerink, S. R. Marder, I. McCulloch, M. Fahlman, S. Fabiano, C. Müller, *Nat. Mater.* **2019**, *18*, 149.

[37] Y. Karpov, T. Erdmann, I. Raguzin, M. Al-Hussein, M. Binner, U. Lappan, M. Stamm, K. L. Gerasimov, T. Beryozkina, V. Bakulev, D. V Anokhin, D. A. Ivanov, F. Günther, S. Gemming, G. Seifert, B. Voit, R. Di Pietro, A. Kiriy, *Adv. Mater.* **2016**, *28*, 6003.

[38] S. Siahrostami, A. Verdaguer-Casadevall, M. Karamad, D. Deiana, P. Malacrida, B. Wickman, M. Escudero-Escribano, E. A. Paoli, R. Frydendal, T. W. Hansen, I. Chorkendorff, I. E. L. Stephens, J. Rossmeisl, *Nat. Mater.* **2013**, *12*, 1137.

[39] Y.-S. Ye, J. Rick, B.-J. Hwang, Y.-S. Ye, J. Rick, B.-J. Hwang, *Polymers (Basel).* **2012**, *4*, 913.

[40] N. A. Anastasijević, V. Vesović, R. R. Adžić, *J. Electroanal. Chem.* **1987**, *229*, 305.

[41] P. D. Josephy, T. Eling, R. P. Mason, *J. Biol. Chem.* **1982**, *257*, 3669.

[42] S. T. Keene, A. Melianas, Y. van de Burgt, A. Salleo, *Adv. Electron. Mater.* **2019**, *5*, 1800686.

[43] E. Mitraka, M. J. Jafari, M. Vagin, X. Liu, M. Fahlman, T. Ederth, M. Berggren, M. P. Jonsson, X. Crispin, *J. Mater. Chem. A* **2017**, *5*, 4404.

Supporting Information

The supporting information contains the synthesis and characterization of p(gPyDPP-MeOT2) and p(gPyDPP-T2), electrochemical characterization, spectroelectrochemical measurements, DFT

calculations, GIWAXS measurements, FT-IR and XPS measurements, OECT measurements, RRDE measurements and enzymatic detection of hydrogen peroxide.

Figures

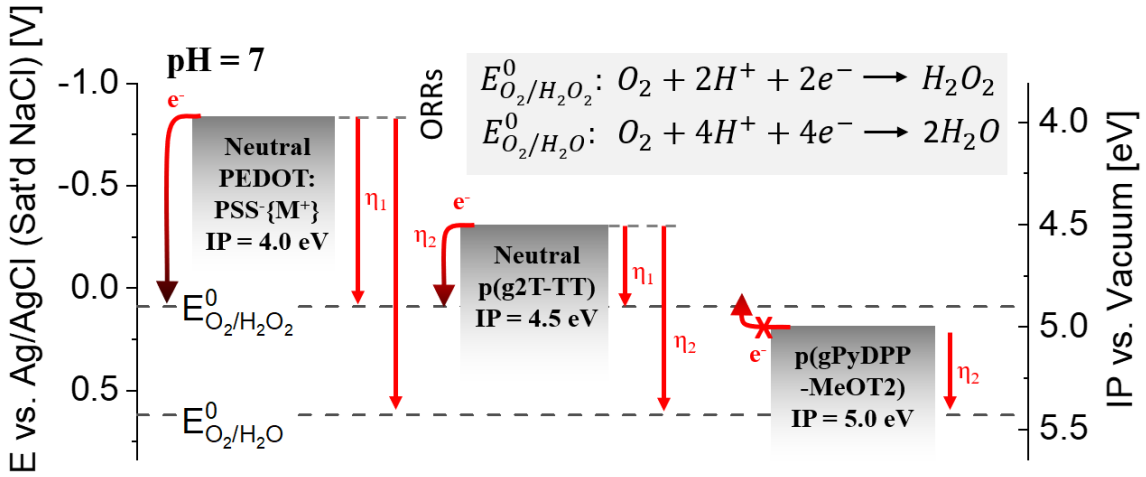

Figure 1. a) Schematic relating the energy levels of the OMIECs, using the IPs of the neutral OMEICs, to the standard electrode potentials for the ORRs with i) two-electron ORR reaction ($O_2 + 2H^+ + 2e^- \rightarrow H_2O_2$, E^0 = 0.70 V vs. RHE, pH = 7-11.7 , E = ~0.1 V vs. Ag/AgCl, for pH = 7) and ii) four-electron ORR reaction ($O_2 + 2H_2O + 4e^- \rightarrow 4OH^-$, E^0 = 1.23 V vs. RHE, pH = 7, E = ~0.6 V vs. Ag/AgCl, for pH = 7). Although the four-electron reaction is thermodynamically more favorable than the two-electron reaction, the rate for the reaction can be low due to the slow kinetics of the reactions. η represents the free energy difference between the reactants and the reaction products (η_1 for the H_2O_2 pathway and η_2 for the H_2O pathway) and the sign of η determines whether the reaction is exergonic (η > 0) or endergonic (η < 0). The two-electron ORR (product H_2O_2) is endergonic for OMIECs with IPs > 4.9 eV (oxidation onsets at potentials > 0.15 V vs Ag/AgCl, pH = 7) and hence prevent the OMIEC from undergoing ORR that form H_2O_2. We note that the mechanism of the ORR is more complicated than described in the simplified picture and can proceed via several intermediates.[22]

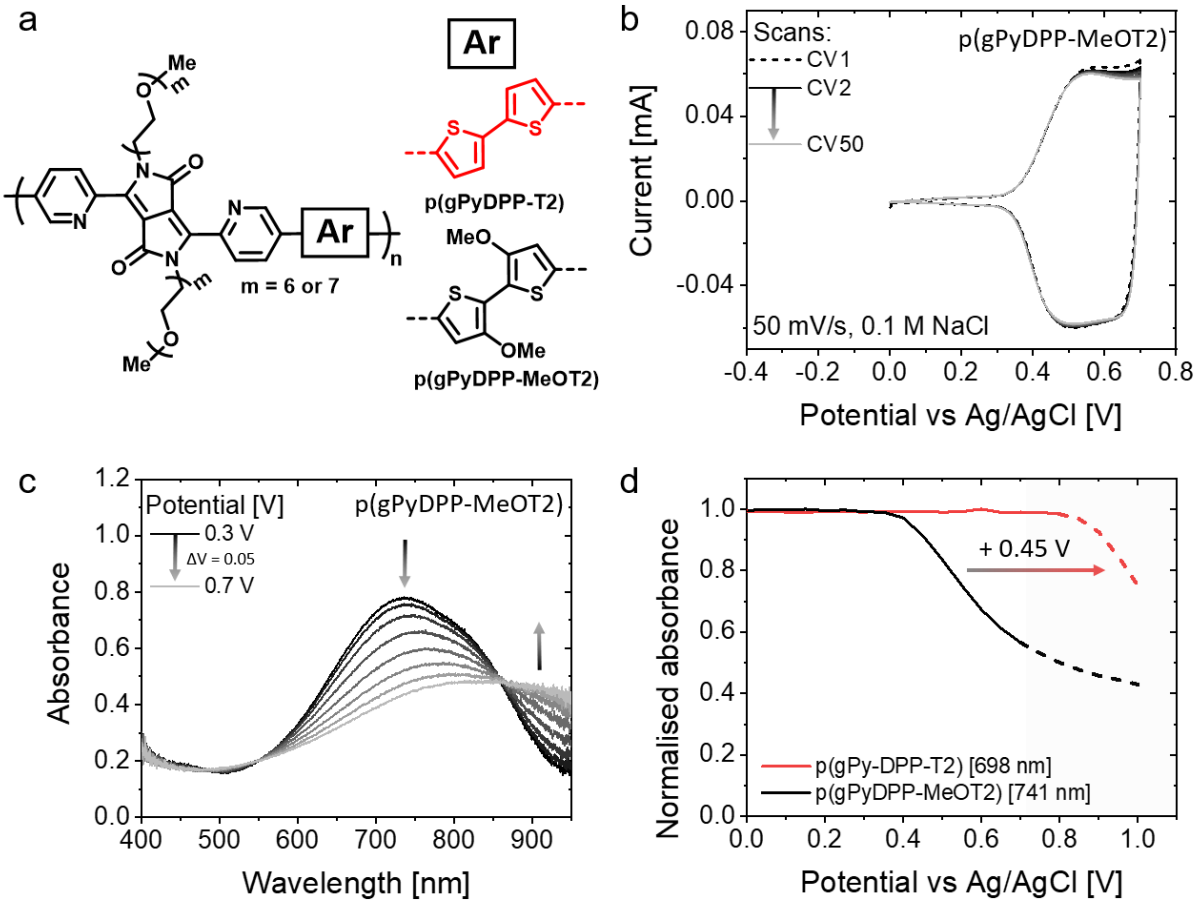

Figure 2. Characterization of the copolymers. a) Chemical structure of the copolymers p(gPyDPP-T2) and p(gPyDPP-MeOT2). b) CV measurements of p(gPyDPP-MeOT2) deposited on ITO-coated glass substrates with a scan rate (ν) of 50 mV/s in 0.1 M NaCl vs. Ag/AgCl, showing 50 scans. c) Spectroelectrochemical measurements of p(gPyDPP-MeOT2) during the charging of the film with voltage steps of 0.05 V from 0.3 V to 0.7 V vs. Ag/AgCl. d) Electrochemical redox stability of p(gPyDPP-T2) and p(gPyDPP-MeOT2), plotting changes of the absorption spectrum (λ_{max}) during the charging of the polymers to 1.0 V vs. Ag/AgCl in 0.1 M NaCl aqueous solution. Additional information is provided in section 9 of the Supporting Information.

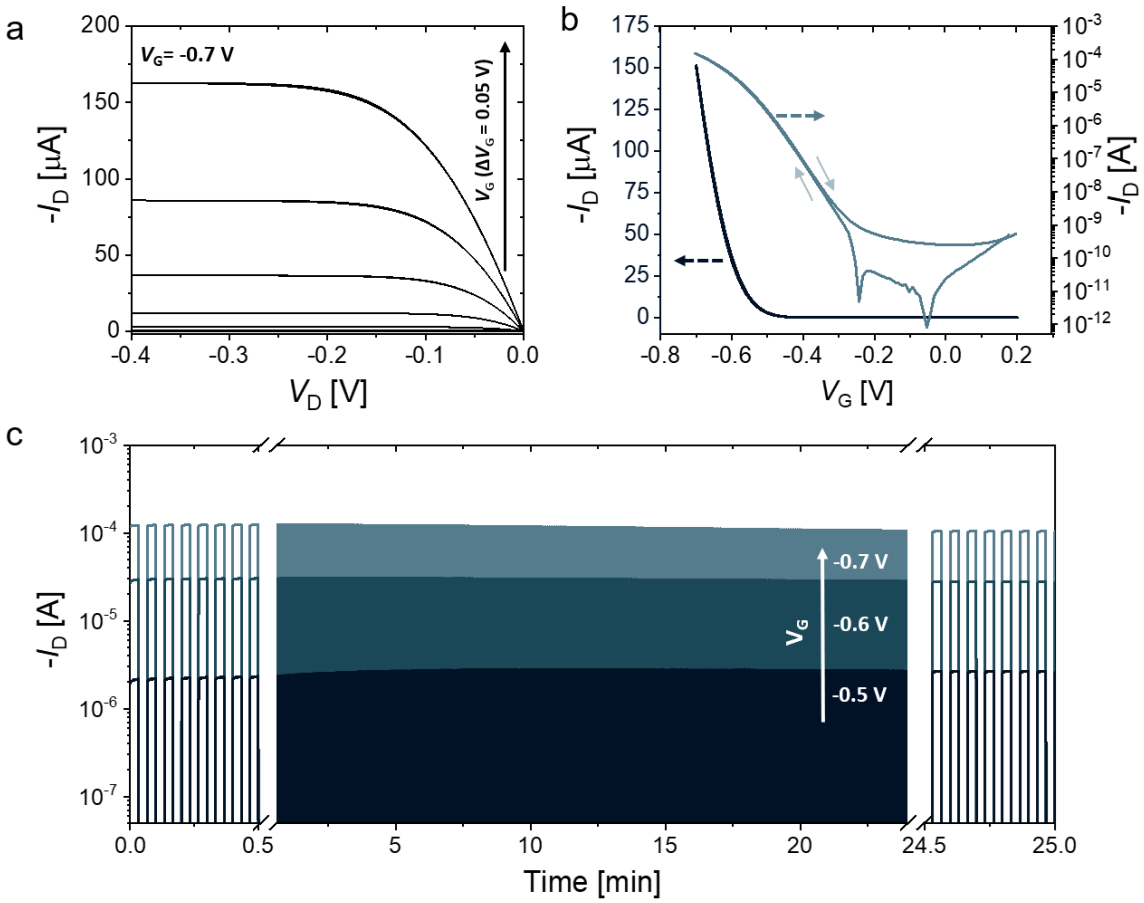

Figure 3. OECT performance of p(gPyDPP-MeOT2) in 0.1 M NaCl aqueous electrolyte in ambient conditions with W = 100 µm, L = 10 µm, and d = 120 nm. a) Output curve (V_G = 0 V to – 0.7 V, ΔV_G = 0.05 V, ν = 0.1 V s^{-1}), b) transfer curve (V_D = – 0.4 V, ν = 0.1 V s^{-1}) (including the gate currents (Figure S37)) and c) stability pulsing experiment by applying alternating the gate potentials between V_G = 0 V and (i) V_G = -0.5 V, (ii) V_G = – 0.6 V or (iii) V_G = – 0.7 V (with V_D = – 0.4 V) with a pulse duration of 2 s. The device was operated for 25 minutes, where I_D is highlighted at the beginning and the end of the experiment (additional long-term stability measurements are provided in Figure S23, Supporting Information).

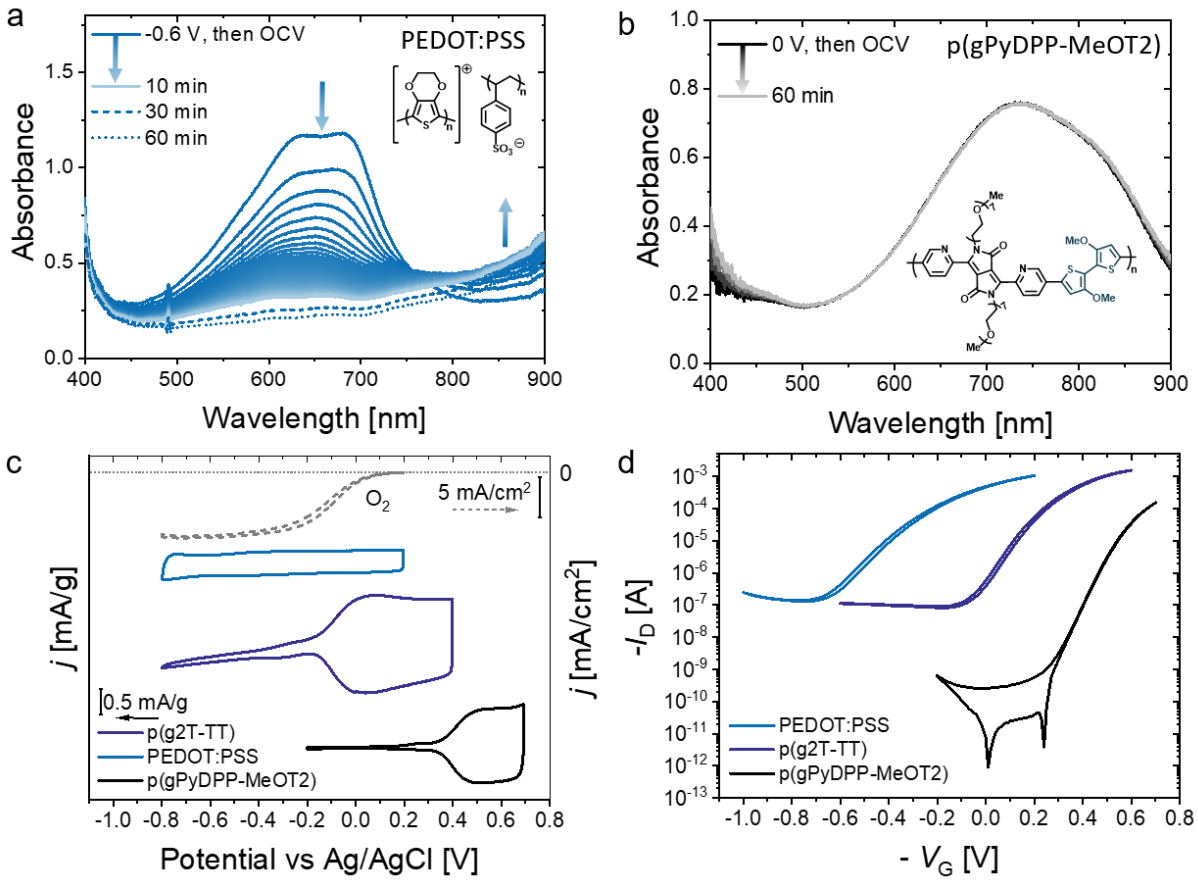

Figure 4. Spectroelectrochemical and electrochemical measurements of the polymer series. Monitoring changes of the absorption spectrum (oxidation of the polymer due to ORRs) for a) PEDOT:PSS after discharging the polymer at – 0.6 V vs. Ag/AgCl for 100 s and switching to OCV conditions and b) p(gPyDPP-MeOT2) after applying 0 V vs. Ag/AgCl for 100 s and switching to OCV conditions (note, the polymer has no redox states at 0 V as shown in Figures 2b-c). c) Cyclic voltammograms of PEDOT:PSS, p(g2T-TT), p(gPyDPP-MeOT2) using a rotating-disk electrode rotating at 1600 RPM at low oxygen concentration vs. Ag/AgCl (Figure S39b, Supporting Information, for CV measurement performed at saturated oxygen concentration) and monitoring the ORR at a rotating Pt ring-electrode at saturated oxygen concentration in 0.1 M NaCl aqueous solution vs. Ag/AgCl (ν = 5 mV s^{-1}). d) Transfer curve of OECTs showing PEDOT:PSS (V_D = – 0.1 V, ν = 1 V s^{-1}), p(g2T-T) (V_D = – 0.3 V, ν = 1 V s^{-1}), p(gPyDPPMeOT2) (V_D = – 0.2 V, ν = 1 V s^{-1}) with 0.1 M NaCl in ambient conditions. W = 100 µm and L = 10 µm for all devices.

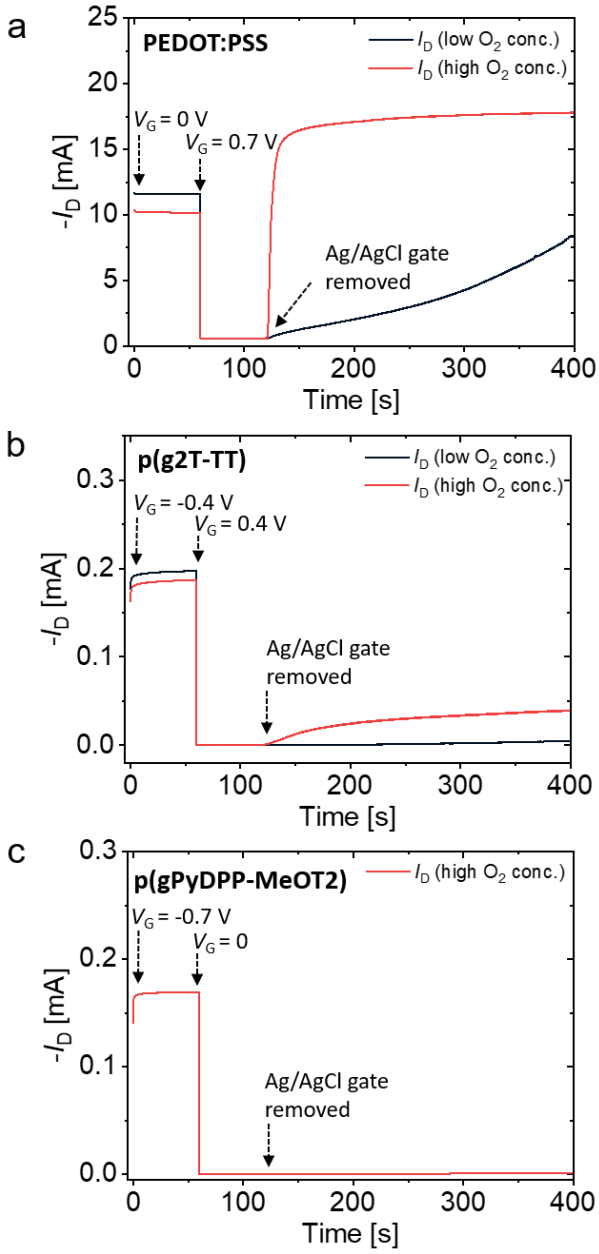

Figure 5. OECT performance in ambient and inert conditions. a) OECT performance of PEDOT:PSS, applying gate potentials of V_G = 0 V or V_G = 0.7 V for 60 s (with V_D = – 0.5 V) before switching to OCV in inert conditions (black line) and ambient conditions (red line), in agreement with results reported for PEDOT:Cl.[43] b) OECT performance of pg2T-TT, applying gate potentials of V_G = – 0.4 V or V_G = 0.4 V for 60 s (with V_D = – 0.5 V) before switching to OCV in inert conditions (black line) and ambient conditions (red line). c) OECT performance of p(gPyDPP-MeOT2) in ambient conditions, applying gate potentials of V_G = – 0.7 V for 60 s or V_G = 0 V (with V_D = – 0.2 V) before switching to OCV in ambient conditions.

TOC

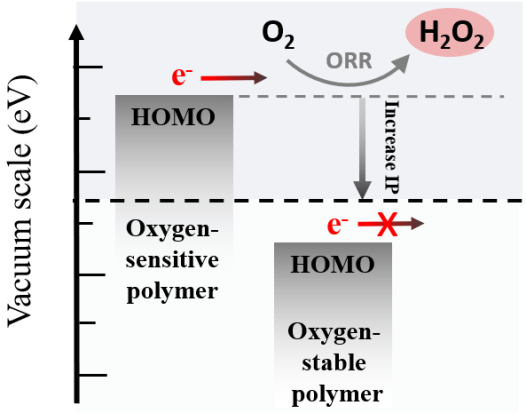

Faradaic side-reactions of redox-active materials, that can produce harmful side products, should be minimized when employed in bioelectronic devices for studying biological systems. This work sheds light on side reactions with molecular oxygen in state-of-the-art materials for electrochemical transistors, forming hydrogen peroxide (H_2O_2), and provides design rules towards high-performance materials that prevent adverse reactions by tailoring the energy levels of the redox-active material.

Faradaic side-reactions of redox-active materials, that can produce harmful side-products, should be minimized when employed in bioelectronic devices for studying biological systems. This work sheds light on side-reactions with oxygen in state-of-the-art materials for electrochemical transistors, forming hydrogen peroxide (H_2O_2), and provides design rules towards high-performance materials that prevent adverse reactions by tailoring the energy levels of the redox-active material.